JACS
JOURNAL OF THE AMERICAN CHEMICAL SOCIETY

Article

pubs.acs.org/JACS

# Utilizing Photocurrent Transients for Dithiolene-Based Photodetection: Stepwise Improvements at Communications Relevant Wavelengths

Simon Dalgleish,*[,†] Michio M. Matsushita,[†] Laigui Hu,[†,‡] Bo Li,[†,‡] Hirofumi Yoshikawa,[†] and Kunio Awaga*[,†,§]

[†]Department of Chemistry and Research Centre for Materials Science, Nagoya University, Furo-cho, Chikusa, 464-8602 Nagoya, Japan

[‡]Department of Applied Physics, Zhejiang University of Technology, Hangzhou 310023, China

[§]CREST, JST, Nagoya University, Furo-cho, Chikusa, 464-8602 Nagoya, Japan

Supporting Information

**ABSTRACT:** Photodetection based on *bis*-(4-dimethylaminodithiobenzil)-Ni(II) (BDN), a representative and well-studied metal dithiolene that shows strong absorption in the near-infrared region of the electromagnetic spectrum, has been investigated. By adopting a metal/insulator/semiconductor/metal (MISM) structure, the peak photocurrent response to an oscillating light chain is increased by up to 50 times, compared to devices without an insulating layer. The transient form of the MISM photoresponse, while unsuitable for steady-state photodetection, can be used to detect periodic light signals of frequencies up to 1 MHz, and is thus applicable for optical communication. Further improvements have been realized by nanostructuring carbon black into the dithiolene layer, improving charge collection, and yielding detectivity of up to $1.6 \times 10^{11}$ Jones at wavelengths beyond the scope of silicon photodiodes. Such an architecture may allow the favorable absorption properties of other such metal dithiolenes to be harnessed, where their low charge carrier mobilities and short excitation lifetimes have previously limited their applicability to this field.

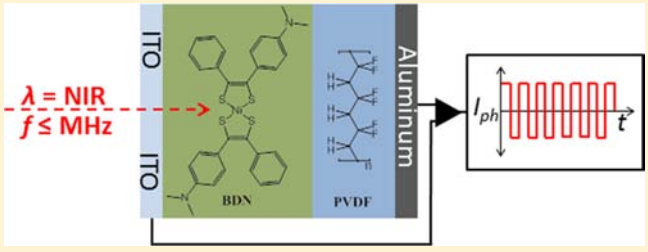


## 1. INTRODUCTION

The field of organic (opto)electronics has seen substantial, and still growing, interest over the past 40 years.[1,2] This attention has resulted in significant improvements in charge carrier mobilities for devices such as transistors and quantum efficiencies for light-to-energy conversion (LEC).[3,4] While these figures of merit remain lower than for inorganic devices, the field is supported by a host of secondary benefits, such as lightweight materials, tunability of the organic component(s), and perhaps most importantly, solution processability, allowing for cheap and flexible devices to be realized.

Compared to organic solar cells, organic photodetectors have received relatively little attention, despite the obvious benefit of precise wavelength targeting of the organic materials. Previous research has focused on tuning the wavelength of the photoabsorber within conventional solar cell architectures, with few notable exceptions.[5−9] However, in order to optimize organic photodetection, attention must be paid to the differences in purpose rather than the similarities. While organic solar cells require high efficiencies, organic photodetectors must show high detectivity (similar to ON/OFF ratio). Whereas organic solar cells must achieve high LEC at steady-state, organic photodetectors must achieve high LEC only for the duration of the input signal which for application to communication is generally very short. Finally, organic photodetectors must respond quickly to the input signal in order to achieve high bandwidth data transfer.

Current telecommunications technology is based on silica fiber optics, which are most transparent in the near-infrared (NIR) region of the electromagnetic spectrum.[10] Within this region, square planar metal *bis*-dithiolenes (hereafter referred to as dithiolenes) are unmatched in their ability to be systematically tuned to absorb light between 700 and 1600 nm by rational modification of the metal, the ligand(s), and the charge of the complex.[11−14] Only recently have dithiolenes begun to be explored as electronic materials, and some have shown reasonably balanced ambipolar mobilities ($\mu$), reaching $10^{-4}$ $cm^2\ V^{-1}\ s^{-1}$.[15] Previous attempts have been made to investigate their optoelectronic application at such wavelengths.[16,17] However, while photocurrent could be generated in the NIR region, cell efficiencies were generally low, and their response speed was limited by the low charge carrier mobilities of the dithiolene component. Thus, a new approach appears necessary to achieve high detectivity while simultaneously achieving fast signal response.

**Received:** May 10, 2012
**Published:** June 25, 2012

   dx.doi.org/10.1021/ja304228c | J. Am. Chem. Soc. 2012, 134, 12742−12750

A recent development in the field of organic optoelectronics is the incorporation of dielectric materials into devices either as blended components[18,19] or as distinct layers.[20,21] While organic semiconductors generally show high exciton binding energies that limit charge separation/extraction, and pose design restrictions on photovoltaic devices, organic materials are inherently more polarizable than inorganic materials, and the local electric fields generated by the dielectrics can aid charge separation/extraction, leading to improvements in LEC for organic optoelectronic devices.[20,22] For devices such as photodetectors, dielectric materials offer an additional benefit by decreasing the dark current that flows through the device, thus increasing its detectivity if the light-on current can be maintained.

In this contribution, photodetectors based on *bis*-(4-dimethylaminodithiobenzyl)-Ni(II) (BDN),[23] which has previously been characterized as an ambipolar semiconductor, with balanced hole and electron mobilities of $\mu \approx 10^{-4}$ cm$^2$ V$^{-1}$ s$^{-1}$,[15] and which shows strong absorption in the NIR ($\varepsilon = 2.8 \times 10^4$ M cm$^{-1}$, $\lambda_{MAX}$ = 1060 nm),[24] have been investigated. Initially, a simple Schottky device architecture (metal/semiconductor/metal) was studied, and on the basis of the photoresponse characteristics of this device, rational improvements were made through incorporation of an appropriate dielectric layer (metal/semiconductor/insulator/metal), which significantly increased the photoresponse of the device. Due to the transient nature of the photoresponse (*vide infra*), the speed of recovery of such devices was also increased, allowing for higher frequency signal detection. Further improvements in efficiency were subsequently achieved by nanostructuring a carbonaceous electrode material into the dithiolene active layer.

## 2. DEVICE FABRICATION

1,1,2-Trichloroethane (TCE) proved an ideal solvent for the spin-coating of large-area thin films of BDN that were free from defects. It should be noted that spinning from chloroform, which has been used in previous studies for transistor characterization, failed to yield homogeneous films over sufficiently large areas.

Figure 1 shows the absorption spectra of the spin-coated films investigated in this study, compared to the solution absorption spectrum of BDN in dichloromethane (DCM). Films of thickness $d$ = 20 and 50 nm, formed by spinning a 10 mg/mL TCE solution of BDN at speeds of 3000 and 1000 rpm, respectively, showed a pronounced red shift in the NIR absorption (872 cm$^{-1}$), with an absorption maximum $\lambda_{MAX}$ = 1168 nm (Figure 1, blue and green lines for 20 and 50 nm thick films, respectively, compared to red line for BDN in solution). The film thickness could be reproducible tuned between 50 and 10 nm (measured by profilometry to an accuracy of ±5 nm), by spinning at speeds greater than 1000 rpm, with no observable change in film quality or relative shape of the absorption spectra. The films appeared smooth by scanning electron microscopy (SEM) (Figure S1a, SI), and showed no observable peaks by thin-film X-ray diffraction on a range of substrates, suggesting that the formed films were amorphous in nature.

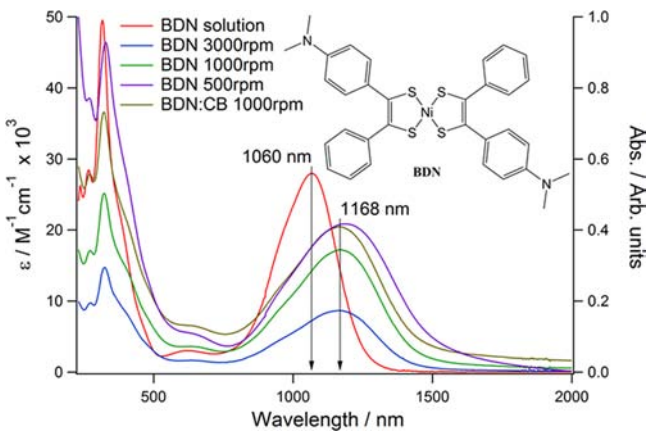


**Figure 1.** UV/vis/NIR spectra of BDN in dichloromethane (DCM) solution, and as single component thin films spin-cast from a 10 mg/mL 1,1,2 TCE solution at speeds of 500, 1000, and 3000 rpm, or as a blend film with carbon black (CB) spun at 1000 rpm (vide infra); (inset: structure of BDN).

For films thicker than 50 nm, formed by either slower spinning, or higher concentration, the $\lambda_{MAX}$ showed a more appreciable red-shift (1045 cm$^{-1}$, Figure 1, purple line) to 1192 nm, as well as a shift in the peaks in the UV region, and a decrease in the relative NIR absorption. Such a red-shift in the solid-state absorption spectra of organic semiconductors, compared to their solution spectra, is a common phenomenon, indicative of increased Coulombic interaction of the molecules with their surroundings.[25] Thus, the greater red-shift in the NIR absorption for films thicker than 50 nm suggests greater crystallinity in such films, compared to those spun at higher speed. This was verified by SEM, which showed a change in the film morphology for the thicker films, displaying an abundance of crystallites over the substrate (Figure S1b, SI). However, the thicker films were also less homogeneous, and proved unsuitable for reproducible device fabrication.

## 3. SCHOTTKY-TYPE DEVICE

For a simple Schottky-type photodetector, the active layer must be sandwiched between two electrodes, at least one of which must be transparent to allow the direct photoexcitation of the active area (the area of electrode superposition).[26] The choice of transparent electrode materials is rather limited, and is currently the subject of extensive research efforts.[27] Indium-doped tin oxide (ITO) is a popular choice, as it is commercially available as patterned electrodes on a range of substrates, and is transparent over a large region of the visible spectrum. However, its transparency in the NIR, especially at wavelengths >1200 nm can fall to less than 70% (*vide infra*), which would have a significant impact on the external quantum efficiency of devices operating in the second and third telecommunications windows (1300 and 1550 nm, respectively). However, for the present study, its transparency in the region of interest proved sufficient.

For passive operation, the electrodes must be of dissimilar work function ($\phi$), thus setting up a potential difference across the device, which facilitates the extraction of charge carriers.[26] Additionally, at least one of the electrodes must be of sufficient energy difference to the frontier orbitals of the semiconductor that a potential (Schottky) barrier is developed to separate the excitons formed upon photoexcitation.[28]

The frontier orbitals of BDN are estimated to be 5.2 and 4.3 eV for the HOMO and LUMO, respectively, derived from its electrochemical and absorption data.[15] Therefore, the formation of a Schottky barrier can be expected at a BDN/ITO interface (assuming a work function $\phi$ = 4.8 eV for ITO).[29] Schottky-type devices were fabricated on ITO by spin-coating from TCE to yield a film thickness of 50 nm and then


dx.doi.org/10.1021/ja304228c | J. Am. Chem. Soc. 2012, 134, 12742−12750

depositing an aluminum electrode by vacuum vapor deposition (thickness $d$ = 100 nm) to give a structure ITO/BDN50 nm/Al. Schottky devices based on thinner BDN films showed significant pin-holing due to penetration of the aluminum through the active layer.

Figure 2 shows the photoresponse of a Schottky-type device to a train of 1050 nm light pulses lasting 5 ms, with a repetition

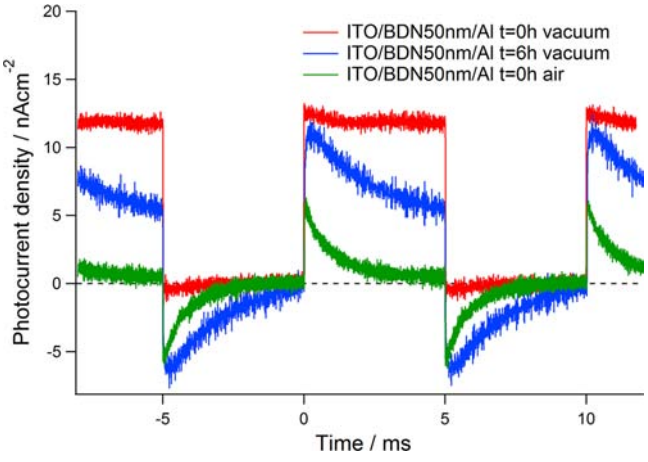


**Figure 2.** Photoresponse of ITO/BDN50 nm/Al photocell to a square-wave light chain at $\lambda$ = 1050 nm ($P_{opt}$ = 1.69 mW cm$^{-2}$, $f$ = 100 Hz), tested *in vacuo* as formed (red), after prolonged testing (blue), and compared to a pristine device tested in air (green).

period of 10 ms (LED $\lambda_{MAX}$ = 1050 nm, $P_{MAX}$ = 1.69 mW cm$^{-2}$, $f$ = 100 Hz), under different experimental conditions. The formed devices showed rapid deterioration of the photoresponse under illumination in air (Figure 2, green line). Such deterioration was not observed when the devices were tested *in vacuo* (Figure 2, red line). For NIR photodetection, testing under vacuum posed significant alignment issues, often resulting in highly variable results. In order to overcome this problem, the devices could be sealed by encapsulation in parylene-C, which improved their air stability, and allowed the devices to be tested under ambient conditions.

The responsivity ($R_i$) of the parylene-coated Schottky devices was calculated using the equation:

$$R_i = \frac{I_{ph}}{P_{opt}} = \frac{q \cdot \lambda \cdot \mathrm{EQE}}{hc} \quad (1)$$

where $I_{ph}$ is the photocurrent response, $P_{opt}$ is the input power, $hc/\lambda$ is the photon energy, $q$ is the elementary charge, and EQE is the external quantum efficiency. The devices showed limited light-to-energy conversion, with a maximum responsivity $R_i$ = 7 ± 2 $\mu$A W$^{-1}$ at 1050 nm (similar to the best performing devices in vacuum). Despite the observation of pin-holing for thinner devices, the reproducibility of devices of active layer thickness $d$ = 50 nm was reasonable. The responsivity was calculated as the weighted mean of four samples (2 devices of 2 pixels each), and the large error (~30%) was attributable to the poor signal-to-noise ratio of the measured photoresponse, and thus, the reproducibility of the devices lay within the precision of the measurement setup. It should be noted that the deviation between pixels was similar to that between devices.

Upon prolonged testing, the photocurrent response to a square-wave light chain changed in form from square-wave to a transient peak of similar magnitude to the initial waveform, followed by a reduced steady-state value (Figure 2, blue line). Upon light-off, the waveform displayed a smaller negative transient, followed by a return to the dark-current level. This effect was also observed upon testing *in vacuo*. Such a change in the waveform could be due to a deterioration of the bulk film, reducing the mobility of the charge carriers through the film. This would result in a buildup of charge in the film upon further photoexcitation, causing space-charge effects.[30,31] Upon light-off, the redistribution of charges in the device would yield a negative spike in the waveform, before settling to a resting state. An alternative explanation could lie in the well-documented aging process of aluminum in the presence of residual oxygen.[32−34] The effect of such a process would be to reduce the steady-state photoresponse of the device through the formation of a highly insulating oxide layer.

The red line in Figure 3 shows the ultrafast photoresponse characteristics of the ITO/BDN50 nm/Al photocell, measured

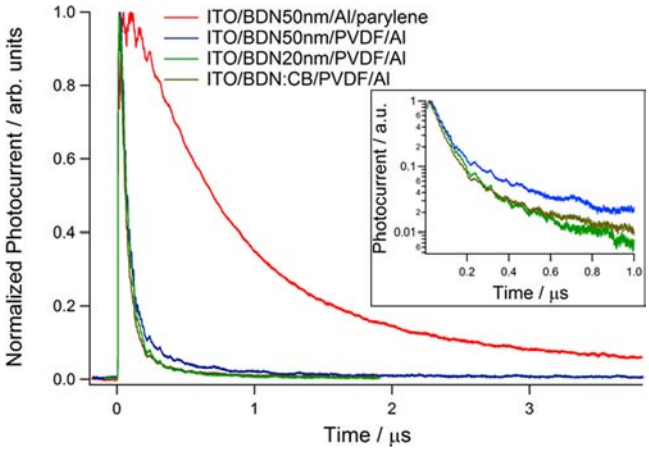


**Figure 3.** Ultrafast photoresponse profile for devices of different architectures to a 1 ns pulsed laser ($\lambda$ = 1064 nm, $f$ = 100 Hz). Inset: Normalized decay kinetics of transient-type devices plotted on a log−linear scale.

using a nanosecond pulsed laser of wavelength $\lambda$ = 1064 nm ($R_{i,1064}$ = 98% of $R_{i,MAX}$), and frequency $f$ = 100 Hz, with the device connected directly to an oscilloscope with a load resistance of 50 Ω. The photoresponse showed a slow decay after photoexcitation, with a response decay time constant $\tau$ = 771.6 ± 0.4 ns. By transforming the decay profile into the frequency domain by fast Fourier transform (FFT), the electrical bandwidth (i.e. the frequency at which the electrical power drops to half (−3 dB) of the dark current value) is ~160 kHz.

These figures of merit are significantly lower than those of commercial photodetectors (e.g. $R_i$ = 0.5 A W$^{-1}$ with cutoff frequency = 1 GHz for a Hamamatsu5973 Si photodetector),[35] and are well below the levels of any practical use. The poor performance is likely due to the poor charge separation and extraction within the device, despite the strong, wavelength-targeted absorption of the dithiolene active layer.

## 4. TRANSIENT-TYPE DEVICES

Despite the reduction observed in the steady-state photocurrent upon prolonged testing for the ITO/BDN50 nm/Al photocell, a transient peak of similar magnitude was still maintained. For telecommunications applications, information is transferred by light pulses of a high frequency, meaning the

light pulses are inherently short (<$\mu$s). In which case, the photoresponse would appear as steady state, as a significant buildup of charge would not be accomplished in this time scale. The size of this "pseudo-steady-state" response would therefore be determined by how much charge had managed to redistribute upon light off after the previous light pulse. In this instance, the bulk region of BDN can be thought of as acting as a capacitor, which charges up upon light-on, and discharges upon light-off.[22] With this in mind, improvements in photocurrent response could be envisioned by replacing the bulk region of BDN with a more suitable dielectric, forming a metal/semiconductor/insulator/metal architecture.

We have previously studied the effect of different dielectric layers on the size of photocurrent transient in an MSIM photocell with a zinc phthalocyanine (ZnPc):$C_{60}$ active layer.[20,22] From this study, it is clear that an ideal dielectric would have high capacitance, and a high dielectric constant, since the former would decrease the dark current, improving the detectivity of the photoresponse, and the latter would facilitate improved charge separation in the film. To this end, polyvinylidene fluoride (PVDF), an organic insulating polymer with high dielectric constant ($\varepsilon$ = 7−13),[36] was investigated. In the first instance, a device structure of ITO/BDN50 nm/PVDF200 nm/Al was adopted.

Figure 4 shows the photoresponse of the ITO/BDN50 nm/PVDF/Al photocell (red line), compared to the Schottky-type

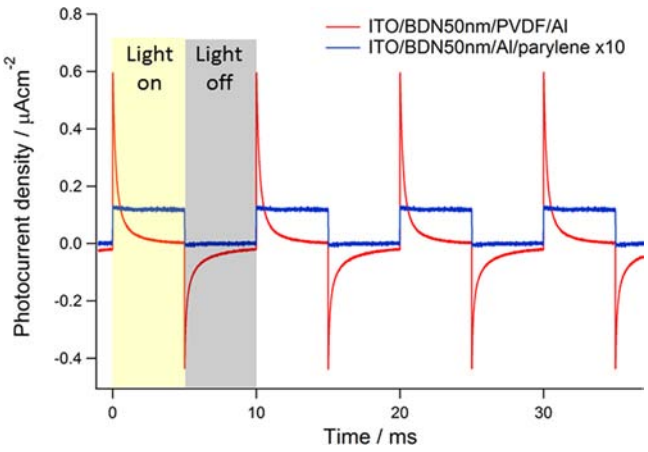


**Figure 4.** Photoresponse of an ITO/BDN50 nm/PVDF/Al photodetector to a square-wave light chain at $\lambda$ = 1050 nm ($P_{opt}$ = 1.69 mW cm$^{-2}$, $f$ = 100 Hz), compared to a parylene-coated ITO/BDN50 nm/Al device (magnified ×10 for clarity).

device (blue line). The incorporation of the PVDF layer is shown to yield up to a 50-fold increase in the peak photocurrent, compared to the single-layer Schottky device, with a maximum responsivity $R_i$ = 0.353 ± 0.009 mA W$^{-1}$ at 1050 nm. This value is calculated as the maximum positive displacement from the dark current level, rather than from the negative peak, and thus represents a significantly lower limit to to the total photoresponse of the device. The devices performed equally well *in vacuo* and under ambient conditions, and thus no additional encapsulation was necessary. Additionally, the reproducibility of the devices was significantly improved, with an error of ∼3% between devices. Due to the improved signal-to-noise ratio, this error describes the variance over the devices. It should be noted that the variance between device batches was greater. Since this is a transient response, it is more sensitive to experimental conditions. One possible source of variance is the difficulty in controlling the PVDF deposition rate, which is known to involve a chain-breaking process.[37] However, the effect of PVDF was always to improve the photoresponse.

Figure 5 shows the frequency dependence of the photoresponse of the ITO/BDN50 nm/PVDF/Al photocell, with the

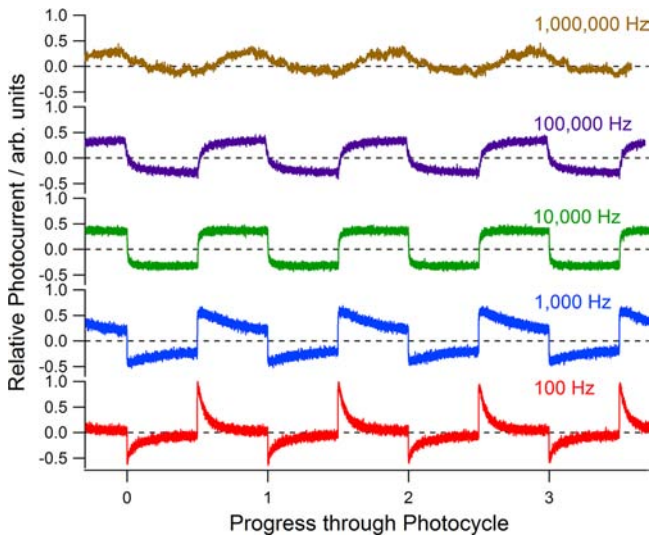


**Figure 5.** Frequency dependence of the photoresponse for an ITO/BDN50 nm/PVDF/Al photocell connected to a high bandwidth (1.6 GHz) current amplifier, tested in air at frequencies from 100 Hz to 1 MHz.

device connected to a high-bandwidth current amplifier (1.6 GHz bandwidth), and illuminated with a square-wave light chain at $\lambda$ = 1050 nm at frequencies between 100 Hz and 1 MHz. At low frequency, the photocurrent waveform shows an initial transient peak that decayed to zero upon light on. On light off, a similar transient peak is observed, though with opposite polarity. The positive and negative peaks are well balanced, suggesting that all the accumulated charge recombines, returning the device to the resting state upon light off. When the frequency was increased, the shape of the waveform changed, as the transient peak did not decay to zero, nor did the recovery process complete before the next signal began. As the frequency increased further, a pseudo-square-wave photoresponse emerged, with a change in polarity for light on and light off conditions. The failure to complete the recovery process results, initially, in a decrease in the size of the photocurrent transient, however, this reduction plateaus, and becomes stable over three decades until a maximum detectable frequency of 1 MHz. The magnitude of the photoresponse at this plateau is still ∼25 times greater than for the simple Schottky-type device.

The ultrafast photoresponse characteristics for the transient-type device, using the pulsed laser, showed superior photoresponse characteristics, with a response decay time constant $\tau$ = 72.6 ± 0.2 ns (Figure 3, blue line). For the Schottky-type device, the response decay time constant was $\tau$ = 771.6 ± 0.4 ns, corresponding to a −3 dB cutoff frequency of ∼160 kHz; therefore, the transient-type device can be expected to show photodetection at frequencies significantly exceeding this limit.

Figure 6 shows the calculated electrical response of the different photodetector architectures as a function of frequency,


dx.doi.org/10.1021/ja304228c | J. Am. Chem. Soc. 2012, 134, 12742−12750

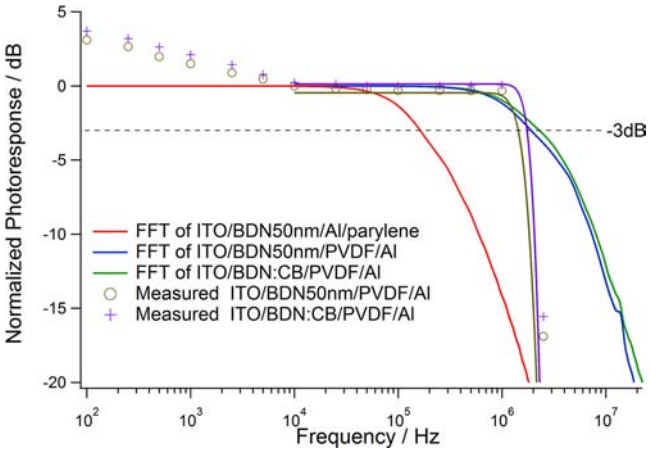


**Figure 6.** Bode plot of the electrical response to a 1 ns laser pulse for the different architecture photodetectors, calculated by FFT from the decay profile of their ultrafast photoresponses, compared to the measured frequency-dependent photoresponses of the transient-type devices.

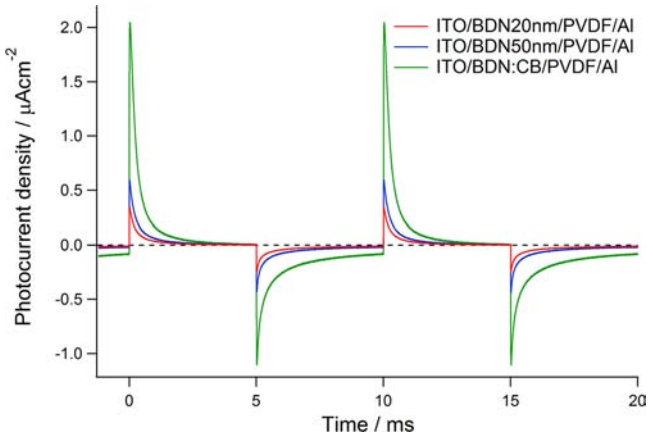


**Figure 7.** Photoresponse of ITO/CB:BDN/PVDF/Al photodetector to a square wave light chain at $\lambda$ = 1050 nm ($P_{opt}$ = 1.69 mW cm$^{-2}$, $f$ = 100 Hz), compared to that of the pure BDN transient-type devices.

compared to their measured frequency-dependent photoresponse. By FFT, the −3 dB cutoff frequency of the transient-type device is calculated to be 1.9 MHz (Figure 6, blue line). Since the cutoff frequency is defined as the frequency at which the response drops to 50% of its dark current value, this point is reached at a frequency of about 5000 Hz, coinciding with the development of a pseudo-steady-state waveform. At this point, the photoresponse stabilizes at this level, persisting to a frequency of about 1 MHz (cf. Figure 5). Due to this unconventional behavior, it may be more appropriate to consider the pseudo-steady-state level as the reference level, and the −3 dB cutoff frequency as the point when the photocurrent drops to half this value, which is ∼1.4 MHz (Figure 6, brown circles). Therefore, despite FFT analysis not taking into account the recovery process of the device, the calculated and measured frequency cutoffs for the transient-type device are very similar. While this approach is perhaps debatable, the ability of the device to detect light signals at frequencies up to 1 MHz is not.

For a single active component device, photocurrent is only expected to be generated in the region close to the metal/semiconductor interface, and this region is relatively narrow for organic semiconductors (<20 nm).[38,39] It could, therefore, be expected that decreasing the active layer thickness would increase the photoresponse, as the built-in potential gradient would be steeper for a thinner device. As discussed earlier, targeting thinner films was not possible for the simple Schottky-type device due to pin-holing; however, the PVDF layer alleviates this problem, highlighting an additional advantage to this structure. However, for devices with a thinner active layer of 20 nm, the photoresponse was only about 60% of that of the transient-type device of 50 nm thick active layer (Figure 7, red line, compared to blue line for 50 nm thick film). It seems, therefore, that charge is harvested from a greater thickness of the film than can reasonably be expected for a simple Schottky junction. In order to understand this, a consideration of a potential mechanism is required. Under short-circuit conditions, the work functions of the ITO and Al electrodes are brought into coalescence, developing a potential gradient over the device. When a dielectric layer is inserted into the device, its greater resistance, compared to that of the active layer, means that the potential difference will be absorbed by the dielectric, and it will become polarized.[40] This polarization may aid charge separation in the active layer, thus facilitating the harvesting of a greater amount of charge carriers within the device, increasing the photoresponse. Accordingly, increasing the dielectric constant of the insulator, which is a measure of the polarizability of a material, should increase the photoresponse for a given film thickness.[20] Therefore, PVDF, with its high dielectric constant, is a good choice for the insulating layer. Moreover, the partial solubility of BDN in most organic solvents, and its observed thermal sensitivity, means that the choice of dielectric materials that can be incorporated into such an architecture is limited to those that can be vapor processed under mild conditions.

## 5. NANOSTRUCTURED DEVICES

Having rationally improved the photoresponse through incorporation of an appropriate dielectric layer, we focused our attention on the active layer. Nickel dithiolenes commonly suffer a short excitation lifetime. Such complexes have previously been modeled using a five level system,[41] where fast intersystem crossing, facilitated by the metal center, accounts for the fast recombination. As a result, the excited state lifetime of BDN has been shown to be of the order of 10 ns.[24] This is expected to limit its light-to-energy conversion, as only the exitons generated at, or very close to, a sufficient energy gradient would be able to dissociate, and those formed at a greater distance would not have sufficient time to drift to such a region before recombination.

Several recent reports have shown that improved light-to-energy conversion can be achieved by nanostructuring carbon nanotubes (CNTs) within the active layer.[42,43] It is thought that the excellent conductive properties of the nanotubes facilitate fast charge extraction from deep within the film. In our hands, however, nanostructured blend films could not be achieved. While the nanotubes dispersed reasonably well in TCE, addition of BDN caused irreversible flocculation, resulting in highly inhomogeneous films, even after ultra-centrifugation. The nature of this interaction is currently under study to determine whether such a CNT−dithiolene interaction can be exploited for optoelectronic application. However, for the present study, the formed films were unsuitable for reproducible device analysis.


dx.doi.org/10.1021/ja304228c | J. Am. Chem. Soc. 2012, 134, 12742−12750

Another common carbonaceous electrode material is carbon black (CB). Although less structurally defined, it is cheap, nanosized, and conductive. CB could be dispersed in TCE and remain as a stable suspension after addition of BDN. After ultracentrifugation, high quality, homogeneous films could be spun and incorporated into devices. The heterogeneous films showed an absorption profile and $\lambda_{MAX}$ similar to those of pure BDN; however, the absorption showed an 18% increase, consistent with a film thickness increase to ∼60 nm, as measured by surface profilometry (Figure 1, brown line). From a control experiment of pure BDN under identical preparation conditions, this was shown not to be due to a concentration increase due to solvent evaporation during ultrasonication but rather to a viscosity increase caused by the dispersed CB.

Figure 7 shows the photoresponse profile of the ITO/CB:BDN/PVDF/Al composite device (green line), compared to the pure BDN transient-type devices. The composite device showed a ∼3 fold increase in photocurrent response, compared to the ITO/BDN50 nm/PVDF/Al device, reaching 1.214 ± 0.004 mA/W at 1050 nm (Figure 7, green line). The ultrafast photoresponse characteristics for this device, using the pulsed laser, show only a limited improvement in speed, with a response decay time constant $\tau$ = 61.48 ± 0.07 ns (Figure 3 (inset), brown line), and by FFT, the −3 dB cutoff frequency was calculated to be 2.3 MHz (Figure 6, green line). Though better resolved, the measured waveform at frequencies up to 1 MHz were similar in shape and progression to the BDN/PVDF devices, suggesting that the composite devices benefited from an increased yield of charge carrier collection, but not speed (−3 dB cutoff frequency 1.7 MHz, Figure 6, purple markers).

Figure 8 shows the wavelength dependence of the photocurrent transient for the composite device, measured over the whole vis/NIR range using a mechanically chopped monochromated light source ($P_{opt}$ = 2 $\mu$W cm$^{-2}$, $f$ = 350 Hz), with the responsivity calculated from the peak of the photocurrent response. The devices are shown to operate from ∼1350 to 400 nm, with a maximum NIR responsivity slightly blue-shifted from the $\lambda_{MAX}$ of the dithiolene film at ∼1050 nm (Figure 8, green line). When the input light power was adjusted for the light absorbed by the ITO substrate (by multiplying the input light power at each wavelength by the transmittance of the ITO (Figure 8, blue line), cf. eq 1), the responsivity spectrum showed an adjusted maximum at ∼1150 nm (Figure 8, brown line) which closely matched the maximum absorption at 1168 nm (Figure 8, red line). It should be noted that the responsivity using mechanically chopped light was lower than that measured by a square-wave-modulated LED light chain as the chopper imposes a slower rise/fall time on the incident light intensity. The waveform of photoresponse to the chopper-modulated light appeared pseudo-square-wave, even at 350 Hz, and was comparable in responsivity to the square-wave-modulated LED light at 5 kHz, which corresponds to the emergence of a pseudo-square-wave photoresponse to the function generator modulated light.

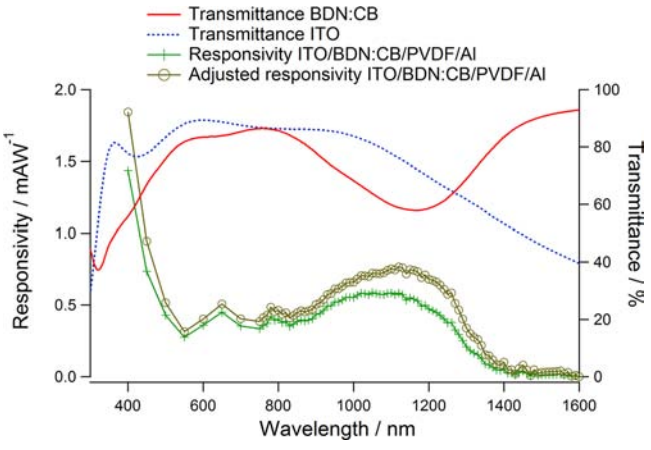


**Figure 8.** Wavelength-dependent responsivity spectra of an ITO/BDN:CB/PVDF/Al device, and spectra adjusted for ITO absorption, illuminated by a tungsten/halogen light source, modulated by mechanical chopper ($P_{opt}$ = <2 $\mu$W cm$^{-2}$, $f$ = 350 Hz), compared to the transmittance spectra of a BDN:CB film on a quartz substrate and the transmittance spectra of an ITO substrate.

## 6. DISCUSSION

For photodetectors, a figure of merit is their noise equivalent power (NEP), which is the optical input power that yields the same output level as the inherent noise level of the detector. It can be calculated from the formula:

$$\mathrm{NEP} = (A\Delta f)^{1/2}/D^* \quad (2)$$

where $A$ is the effective area of the photodetector, $\Delta f$ is the electrical bandwidth in Hz, and $D^*$ is the detectivity, measured in units of Jones. If the dark current ($J_d$) is the dominant intrinsic contribution to the noise, then $D^*$ can be expressed as:

$$D^* = R_i/(2qJ_d)^{1/2} \quad (3)$$

where $R_i$ is the responsivity, $q$ is the elementary charge, and $J_d$ is the dark current. From the measured responsivity at pseudo-steady-state for each device, it can be shown that the detectivity can be systematically increased, reaching a maximum of 1.6 × 10$^{11}$ Jones at 1050 nm for the ITO/CB:BDN/PVDF/Al device (Table 1). This corresponds to an NEP of 1.1 × 10$^{-9}$ W/Hz$^{1/2}$. While these values are poorer than for commercial photodetectors (3 × 10$^{13}$ Jones and 1.1 × 10$^{-15}$ W/Hz$^{1/2}$ for Si, and 5 × 10$^{12}$ Jones and 2.0 × 10$^{-15}$ W/Hz$^{1/2}$ for InGaAs),[35] the devices are shown to operate at wavelengths exceeding that of Si-based detectors, which operate up to 1100 nm and can be easily fabricated from cheap, nontoxic component materials, and furthermore, they operate under passive conditions.

This study serves to demonstrate that significant improvements in responsivity, and speed of response, can be realized for oraganic photodetectors, based on previously unsuitable semiconductors, through the optimization of photocurrent transients. By adopting a metal/semiconductor/insulator/metal (MISM) architecture, the initial photocurrent response is enhanced by the polarization induced in the dielectric by the built-in potential of the device, which improves charge separation in the active layer. Since the charge carriers are not swept through the device, but rather accumulate in the active layer as space charges, the response speed is governed by the speed of recombination, rather than the mobility of the charge carriers. For this reason, BDN, a semiconductor that shows rather low mobilities and a short excited state lifetime but has particularly desirable absorption properties can yield devices with reasonable responsivity and can operate at frequencies up to 1 MHz in a region of the spectra that is particularly relevant to optical communications applications.

While such a device architecture is unsuitable for steady-state optoelectronic devices, the time-varying response to an input light signal can appear pseudo-steady-state if the input signal is

Table 1. Figures of Merit for Different Device Architectures Investigated in This Study

| | $R_i$ (mA W$^{-1}$) | | bandwidth (MHz) | | | |
|---|---|---|---|---|---|---|
| structure | peak | steady-state | FFT | measured | detectability[a] (Jones) | NEP[b] (W/Hz$^{1/2}$) |
| ITO/BDN50 nm/Al | 0.007 ± 0.002 | 0.007 | 0.16 | – | $4.7 \times 10^{7}$ | $1.2 \times 10^{-6}$ |
| ITO/BDN20 nm/PVDF/Al | 0.204 ± 0.004 | 0.108 | – | – | $3.0 \times 10^{10}$ | – |
| ITO/BDN50 nm/PVDF/Al | 0.353 ± 0.009 | 0.181 | 1.9 | 1.4 | $5.0 \times 10^{10}$ | $3.3 \times 10^{-9}$ |
| ITO/BDN:CB/PVDF/Al | 1.214 ± 0.004 | 0.581 | 2.3 | 1.7 | $1.6 \times 10^{11}$ | $1.1 \times 10^{-9}$ |

[a]$D^*$ was calculated on the basis of the (pseudo) steady-state value. [b]NEP was calculated on the basis of the measured bandwidth, where available.

sufficiently short, such as those used in optical communication. Furthermore, the response to each impulse comprises a positive and negative component, with a change in polarity for light-on and light-off conditions, which better helps to resolve the on/off signal modulation.

The incorporation of a dielectric layer in the architecture yields two additional benefits to the devices: it significantly decreases the dark current in the transient-type devices ($J_d$ = 40 pA cm$^{-2}$) compared to the simple Schottky architecture ($J_d$ = 70 nA cm$^{-2}$) (Figure S2, SI), greatly improving the detectivity and NEP, and it insulates the device to atmospheric degradation, which is shown to be an almost instantaneous and irreversible process for the simple Schottky devices.

One common method for increasing the efficiency of charge separation in organic photovoltaic devices is to form a bulk heterojunction[38] with a semiconductor with a HOMO level smaller than (p-type), or a LUMO level greater than (n-type) that of the photoabsorber, thus setting up a p−n junction, with the photoabsorber acting as the n- or p-type semiconductor, respectively. Numerous attempts were made to achieve such a system for BDN. However, all failed to yield an efficiency greater than that of BDN alone, and any photocurrent observed was likely due to a residual ITO/BDN interface, caused by blending. Significant improvements in the efficiency of the transient-type devices could, however, be achieved by blending carbon black into the active dithiolene film. It is thought that the dispersed carbonaceous material provided a greater surface area for charge collection within the film, harvesting charge carriers from deeper within the film than for a planar ITO/dithiolene interface.

This study may provide a means of harnessing the highly desirable NIR absorption properties of metal dithiolenes for optoelectronic application. In order to exploit such materials in the most relevant region of the spectrum for telecommunications applications (1300−1550 nm), some future consideration should be devoted to the choice of electrode materials, since ITO is known to absorb strongly at such wavelengths.

## 7. CONCLUSIONS

Dithiolenes are unmatched in their ability to be rationally tuned to harvest light across the NIR region of the electromagnetic spectrum, which is currently exploited for telecommunications applications. However, their usefulness in optoelectronic devices has been limited by their short excitation lifetimes and low charge carrier mobilities, which adversely affect their responsivity, and speed of operation, respectively, in conventional device architectures. By incorporation of a dielectric layer into a simple Schottky-type device structure, significant improvements in the responsivity and speed of response can be realized. This architecture yields additional benefits in that it significantly decreases the dark current, greatly improving the detectivity of the device, and protects the active layer from atmospheric degradation, allowing the devices to be tested under ambient conditions.

By incorporation of carbon black into the active layer, further improvements in the responsivity can be realized, due to improved charge collection within the device. This simple modification may yield potential improvements to other narrow band gap semiconductors, where suitable heterojunction blend partners cannot be found.

Such simple modifications yield air-stable optoelectronic devices operating at telecommunication wavelengths, with detectivity reaching $1.6 \times 10^{11}$ Jones, and capable of data transfer at rates of up to 1 Mbit s$^{-1}$.

## 8. EXPERIMENTAL SECTION

BDN was synthesized by the general acyloin-$P_4S_{10}$ method of Schrauzer and Mayweg,[24,44] and its purity was confirmed by CHN.

Devices were prepared on patterned ITO substrates (15 mm × 15 mm × 2 mm, with two electrodes defined of width 2 mm), precleaned by sequential ultrasonication (IPA, acetone, chloroform, 10 min each). The active layer was formed by spin-coating a 10 mg mL$^{-1}$ solution of BDN in 1,1,2-TCE for 120 s in air at speeds to yield the desired thickness (confirmed by surface profiling using a Bruker Dektak 150). Processing under nitrogen yielded no perceivable increase in photoresponse. For carbon black (CB)-blended films, a 10 mg/mL solution of BDN in 1,1,2-TCE was added to CB (Tokablack #5500, Tokai Carbon Co., previously dried at 120 °C overnight), to give a CB concentration of 1 mg mL$^{-1}$, and the mixture was ultrasonnicated (400 W, 38 kHz) under cooling for 1 h, whereupon the suspension was centrifuged at 5000 rpm for 10 min to remove larger carbonaceous particles, and films were spin coated from the upper 50% of the supernatant. For the transient-type devices, a layer of PVDF (Sigma-Aldrich) was deposited by vacuum vapor deposition at a rate of 1 Å s$^{-1}$ at an initial vacuum of $3 \times 10^{-4}$ Pa, with its thickness monitored by a quartz-crystal microbalance and confirmed by surface profiling. All devices were completed by deposition of an Al electrode of thickness 100 nm by vacuum vapor deposition (rate of 0.5 Å s$^{-1}$ at an initial vacuum of $3 \times 10^{-4}$ Pa) through a shadow mask, defining an electrode of width 1 mm. For the Schottky devices, encapsulation in parylene-C was achieved using a parylene deposition unit (Specialty Coating Systems PDS2010), forming an insulating film of 200 nm over the devices.

Absorption and transmission spectra were recorded on a Schimadzu UV-3100PC spectrophotometer. Measured films were fabricated under conditions identical to those for the devices on precleaned quartz substrates. Solution absorption measurements were recorded using a quartz cuvette ($L$ = 1 cm) in DCM. Transmission spectra of quartz and ITO were recorded for precleaned substrates.

For testing in air, the devices were mounted in the light path on a holding plate, and connected to the measurement setup using copper wires attached with silver paste. For testing *in vacuo*, the devices were housed in a home-built vacuum chamber with a quartz window (of diameter 8 mm, and transmittance at 1050 nm of 95%) and connected to the measurement setup using copper wires attached with silver paste.

The time- and frequency-dependent transient photocurrent measurements were performed using an LED light source (ThorLabs; $\lambda_{MAX}$ = 1050 ± 50 nm, $P_{MAX}$ = 1.6 mW), powered by a home-built


dx.doi.org/10.1021/ja304228c | J. Am. Chem. Soc. 2012, 134, 12742−12750

driver circuit (circuit diagrams available upon request) and modulated by a function generator (Tektronix AFG320). The light power density was calibrated using an OPHIR NovaII optical power meter.

The wavelength-dependent transient photocurrent measurements were performed using a tungsten/halogen light source (Spectral Products ASBN-W 100 L) with gratings covering the 400−800 nm and 800−1600 nm range, with the light power not exceeding 2 $\mu$W cm$^{-2}$. The monochromated light power density was calibrated by an optical power meter: Adcmt 8230E for the visible range (400−800 nm), and OPHIR NovaII for the NIR range (800−1600 nm). The incident light was mechanically chopped (NF electronic instruments 5584A) at 350 Hz, and the responsivity calculated from the peak of the photocurrent response.

For time and wavelength dependent measurements, the devices were connected to a current amplifier (Keithley 428) in which the transient short circuit current signal was amplified and converted into a voltage signal, which was recorded and averaged to filter noise by an oscilloscope (Tektronix TDS5104B).

For the frequency response measurements, the devices were connected to a home-built high-bandwidth current amplifier (circuit diagram available upon request) (active chip: Texas Instruments OPA657, 1.6 GHz bandwidth) and converted to a voltage signal, which was recorded and averaged by the oscilloscope.

The ultrafast impulse response to a nanosecond laser pulse (CryLas FDSS532-Q2, $\lambda$ = 1064 nm, repetition rate 100 Hz, pulse width 1 ns, pulse energy reduced to 2 $\mu$J using ND filters) was recorded by directly connecting the device to the oscilloscope with an input resistance of 50 Ω.

## ■ ASSOCIATED CONTENT

### Supporting Information

Scanning electron microscope images of formed films and current/voltage measurements of formed devices. This material is available free of charge via the Internet at http://pubs.acs.org.

## ■ AUTHOR INFORMATION


### Corresponding Author

dalgleish.simon.john@j.mbox.nagoya-u.ac.jp; awaga.kunio@b.mbox.nagoya-u.ac.jp


### Notes

The authors declare no competing financial interest.

## ■ ACKNOWLEDGMENTS

This research was financially supported by a Grant-in-Aid for Scientific Research from the Ministry of Education, Culture, Sport, Science and Technology (MEXT) of Japan. L.H. also thanks the National Natural Science Foundation of China (Grant No. 11004172) and Qianjiang Talent Project of Zhejiang Province (Grant No. 2011R10088).

## ■ REFERENCES


(1) Themed Issue on Molecular Conductors Batail, P. *Chem. Rev.* **2004**, *104*, 4887−5782.

(2) Themed issue on Solar Cells Grätzel, M.; Janssen, R. *J. Mater. Chem.* **2009**, *19*, 5276−5451.

(3) Arias, A.; MacKenzie, J.; McCulloch, I.; Rivnay, J.; Salleo, A. *Chem. Rev.* **2010**, *110*, 3−24.

(4) Brabec, C.; Gowrisanker, S.; Halls, J.; Laird, D.; Jia, S.; Williams, S. *Adv. Mater.* **2010**, *22*, 3839−3856.

(5) Peumans, P.; Bulovíc, V.; Forrest, S. *Appl. Phys. Lett.* **2000**, *76*, 3855−3857.

(6) Konstantatos, G.; Clifford, J.; Levina, L.; Sargent, E. *Nat. Photonics* **2007**, *1*, 531−534.

(7) Arnold, M.; Zimmerman, J.; Renshaw, C.; Xu, X.; Lunt, R.; Austin, C.; Forrest, S. *Nano Lett.* **2009**, *9*, 3354−3358.

(8) Binda, M.; Iacchetti, A.; Natali, D.; Beverina, L.; Sassi, M.; Sampietro, M. *Appl. Phys. Lett.* **2011**, *98*, 073303.

(9) Peumans, P.; Yakimov, A.; Forrest, S. *J. Appl. Phys.* **2003**, *93*, 3693−3723.

(10) Desurvire, E.; Kazmierski, C.; Lelarge, F.; Marcadet, X.; Scavennec, A.; Kish, F.; Welch, D.; Nagarajan, R.; Joyner, C., Jr.; R., S.; Corzine, S.; Kato, M.; Evans, P.; Ziari, M.; Dentai, A.; Pleumeekers, J.; Muthiah, R.; Bigo, S.; Nakazawa, M.; Richardson, D.; Poletti, F.; Petrovich, M.; Alam, S.; Loh, W.; Payne, D. *C. R. Phys.* **2011**, *12*, 387−416.

(11) Mueller-Westerhoff, U.; Vance, B.; Yoon, D. *Tetrahedron* **1991**, *47*, 909−932.

(12) Kokatam, S.; Ray, K.; Pap, J.; Bill, E.; Geiger, W.; LeSuer, R.; Rieger, P.; Weyhermüller, T.; Neese, F.; Wieghardt, K. *Inorg. Chem.* **2007**, *46*, 1100−1111.

(13) Deplano, P.; Pilia, L.; Espa, D.; Mercuri, M.; Serpe, A. *Coord. Chem. Rev.* **2010**, *254*, 1434−1447.

(14) Perochon, R.; Davidson, P.; Rouzière, S.; Camerel, F.; Piekara-Sady, L.; Guizouarn, T.; Fourmigué, M. *J. Mater. Chem.* **2011**, *21*, 1416−1422.

(15) Anthopoulos, T.; Setayesh, S.; Smits, E.; Cölle, M.; Cantatore, E.; de Boer, B.; Blom, P.; deLeeuw, D. *Adv. Mater.* **2006**, *18*, 1900−1904.

(16) Aragoni, M.; Arca, M.; Devillanova, F.; Isaia, F.; Lippolis, V.; Manacini, A.; Pala, L.; Verani, G.; Agostinelli, T.; Caironi, M.; Natali, D.; Sampietro, M. *Inorg. Chem. Commun.* **2007**, *10*, 191−194.

(17) Dalgleish, S.; Labram, J.; Li, Z.; Wang, J.; McNeill, C.; Anthopoulos, T.; Greenham, N.; Robertson, N. *J. Mater. Chem.* **2011**, *21*, 15422−15430.

(18) Minami, N.; Sasaki, K.; Tsuda, K. *J. Appl. Phys.* **1983**, *54*, 6764−6766.

(19) Nalwa, K.; Carr, J.; Mahadevapuram, R.; Kodali, H.; Bose, S.; Chen, Y.; Petrich, J.; Ganapathysubramanian, B.; Chaudhary, S. *Energy Environ. Sci* **2012**, *5*, 7042−7049.

(20) Hu, L.; Noda, Y.; Ito, H.; Kishida, H.; Nakamura, A.; Awaga, K. *Appl. Phys. Lett.* **2010**, *96*, 243303.

(21) Yuan, Y.; Reece, T.; Sharma, P.; Poddar, S.; Ducharme, S.; Gruverman, A.; Yang, Y.; Huang, J. *Nat. Mater.* **2011**, *10*, 296−302.

(22) Hu, L.; Awaga, K. Anomalous Transient Photocurrent. In *Optoelectronics: Devices and Applications*; Predeep, P., Ed.; InTech: Rijeka, Croatia, and Shanghai, China, 2011; Chapter 26, pp 553−572.

(23) Drexhage, K.; Mueller-Westerhoff, U. *IEEE J. Quantum Electron.* **1972**, *QE 8*, 759.

(24) Magde, D.; Bushaw, B.; Windsor, M. *Chem. Phys. Lett.* **1974**, *28*, 263−269.

(25) Ostroverkhova, O.; Shcherbyna, S.; Cooke, D.; Egerton, R.; Hegmann, F.; Parkin, R. T. S.; Anthony, J. *J. Appl. Phys.* **2005**, *98*, 033701.

(26) Günes, S.; Neugebauer, H.; Sariciftci, N. *Chem. Rev.* **2007**, *107*, 1324−1338.

(27) Hecht, D.; Kaner, R. *MRS Bull.* **2011**, *36*, 749−755.

(28) Stallinga, P. *Electrical Characterization of Organic Electronic Materials and Devices*; John Wiley and Sons, Ltd.: Chichester, 2009; Front Matter.

(29) Schlaf, R.; Murata, H.; Kafafi, Z. *J. Electron. Spectrosc.* **2001**, *120*, 149−154.

(30) McNeill, C.; Hwang, I.; Greenham, N. *J. Appl. Phys.* **2009**, *106*, 024507.

(31) Hu, L.; Iwasaki, A.; Suizu, R.; Noda, Y.; Li, B.; Yoshikawa, H.; Matsushita, M.; Awaga, K.; Ito, H. *Phys. Rev. B* **2011**, *84*, 205329.

(32) Tsukamoto, J.; Ohigashi, H.; Matsumura, K.; Takahashi, A. *Synth. Met.* **1982**, *4*, 177−186.

(33) Glenis, S.; Horowitz, G.; Tourillon, G.; Garnier, F. *Thin Solid Films* **1984**, *111*, 93−103.

(34) Antoniadis, H.; Hsieh, B.; Abkowitz, M.; Jenekhe, S.; Stolka, M. *Synth. Met.* **1994**, *62*, 265−271.

(35) Hamamatsu Product Calalogue; http://sales.hamamatsu.com/en/products.php; 2011.

(36) Kerbow, D. L.; Sperati, C. A. In *Polymer Handbook*, 4th ed.; Brandrup, J., Immergut, E. H., Grulke, E. A., Eds.; Wiley: New York, 1999; Chapter 5, pp 2−3.
(37) Takeno, A.; Okui, N.; Kitoh, T.; Muraoka, M.; Umemoto, S.; Sakai, T. *Thin Solid Films* **1991**, *202*, 205−211.
(38) Yu, G.; Gao, J.; Hummelen, J.; Wudl, F.; Heeger, A. *Science* **1995**, *270*, 1789−1791.
(39) Scully, S.; McGehee, M. *J. Appl. Phys.* **2006**, *100*, 034907.
(40) Stallinga, P.; Benvenho, A.; Smits, E.; Mathijssen, S.; Cölle, M.; Gomes, H.; de Leeuw, D. *Org. Electron.* **2008**, *9*, 735−739.
(41) Tan, W.; Ji, W.; Zuo, J.; Bai, J.; You, X.; Lim, J.; Yang, S.; Hagan, D.; Stryland, E. V. *Appl. Phys. B* **2000**, *70*, 809−812.
(42) Li, C.; Chen, Y.; Wang, Y.; Iqbal, Z.; Chhowalla, M.; Mitra, S. *J. Mater. Chem.* **2007**, *17*, 2406−2411.
(43) Cataldo, S.; Salice, P.; Menna, E.; Pignataro, B. *Energy Environ. Sci* **2012**, *5*, 5919−5940.
(44) Schrauzer, G.; Mayweg, V. *J. Am. Chem. Soc.* **1965**, *87*, 1483−1489.